DALTON

Structures and luminescent properties of polynuclear gold(I) halides containing bridging phosphine ligands

Hong Xiao,[a] Yu-Xiang Weng,[a] Wing-Tak Wong,[a] Thomas C. W. Mak[b] and Chi-Ming Che*,[a]

[a] *Department of Chemistry, The University of Hong Kong, Pokfulam Road, Hong Kong*
[b] *Department of Chemistry, The Chinese University of Hong Kong, Shatin, New Territories, Hong Kong*

The complexes $[AuI(PPh_3)]$ **1**, $[Au_2(\mu\text{-dppm})Cl_2]$ **2** [dppm = bis(diphenylphosphine)methane], $[Au_2(\mu\text{-dppm})I_2]$ **3**, $[Au_3(\mu\text{-tppm})Cl_3]$ **4** [tppm = tris(diphenylphosphino)methane], $[Au_3(\mu\text{-tppm})I_3]$ **5**, $[Au_3(\mu\text{-dpmp})_2Cl_2]Cl$ **6** [dpmp = bis(diphenylphosphinomethyl)phenylphosphine] and $[Au_3(\mu\text{-dpmp})_2I_2]I$ **7** were prepared. The crystal structures of **5**–**7** have been established by X-ray crystal analysis. The measured intramolecular Au–Au distances are 3.136(1) Å in **5**, 2.946(3) and 2.963(3) Å in **6** and 2.952(1) and 3.020(1) Å in **7**. Extended-Hückel molecular orbital calculations revealed that the 6p orbitals of iodide and 5d orbitals of gold(I) make a significant contribution to the highest occupied molecular orbitals of **5** and of **2** and **4** respectively. The lowest unoccupied molecular orbitals of these complexes mainly comprise π* orbitals of the phosphines. The photophysical properties of **1**–**6** have been studied. All show dual emissions. The low-energy emissions at around 660–680 nm have a small red shift in energy from chloro to iodo complexes, and a much higher intensity at room temperature than at 77 K. These are attributed to triplet states with mixed ^{3}m.m.l.c.t. (metal–metal to ligand charge transfer, gold→phosphine) and ^{3}l.l.c.t. (ligand to ligand charge transfer, halide to phosphine) characters. The high-energy emissions at around 460–530 nm are more prominent at 77 K and assigned to intraligand and or ^{3}m.l.c.t. (metal to ligand charge transfer) transitions. The temperature effects on the luminescence lifetimes of these complexes have also been studied.

There is growing interest in the photophysical properties and photochemistry of luminescent metal clusters, especially those of d^{10} metal ions such as Cu^I,[1] and Ag^I[2] and Au^I.[3–5] In most reports on luminescent d^{10}-metal clusters the effect of metal–metal interaction on both the ground- and excited-state properties has been emphasized. Ford and Volger[1] revealed that metal-cluster-centred excited states have been proposed in some tetranuclear copper(I) clusters. In this laboratory much effort has been directed to the synthesis and photophysical studies of luminescent gold(I) complexes.[3] By systematic variation of the number of gold(I) atoms and the Au–Au separations, a significant effect on the electronic absorption spectra of polynuclear gold(I) complexes containing bridging phosphine ligands has been observed. In most di- and tri-nuclear gold(I) phosphine complexes studied the emitting states were suggested to arise from metal-centred transitions.[3a,c,f]

As part of our continuing program in the study of d^{10}–d^{10} interactions, we here describe the structures and temperature-dependent emission properties of several gold(I) halide clusters with bridging phosphine ligands, $[AuI(PPh_3)]$ **1**, $[Au_2(\mu\text{-dppm})X_2]$ [dppm = bis(diphenylphosphino)methane, X = Cl **2** or I **3**], $[Au_3(\mu\text{-tppm})X_3]$ [tppm = tris(diphenylphosphino)-methane, X = Cl **4** or I **5**] and $[Au_3(\mu\text{-dpmp})_2X_2]X$ [dpmp = bis(diphenylphosphinomethyl)phenylphosphine, X = Cl **6** or I **7**]. Luminescence thermochromism has been observed in these complexes and the lowest emitting excited states are suggested to have mixed ^{3}m.m.l.c.t. (metal–metal to ligand charge transfer) and ^{3}l.l.c.t. (ligand to ligand charge transfer) characters.

Experimental

Materials

The compounds $K[AuCl_4]$, dppm and tppm were obtained from Strem Chemicals, dpmp was prepared by the literature method,[6] triphenylphosphine (Merck) and 2,2′-thiodiethanol (Strem) were used as received and chloro(dimethyl sulfide)gold(I),[7] $[AuI(PPh_3)]$[8] **1** and $[Au_2(\mu\text{-dppm})Cl_2]$[8] **2** were prepared by published procedures. All the solvents for photochemical measurements were purified by repeated distillations. Acetonitrile (Ajax, AR) was distilled from $KMnO_4$ and CaH_2 under nitrogen.

Syntheses

$[Au_2(\mu\text{-dppm})I_2]$ 3. The complex was synthesized by a modification of the literature method.[8] A mixture of $[Au_2(\mu\text{-dppm})Cl_2]$ (0.46 g, 0.59 mmol) and KI (0.8 g, 4.8 mmol) in acetone (150 cm^3) was refluxed for 1 h and subsequently stirred for 24 h at room temperature. Acetone was evaporated and the solid residue washed with water. White crystals (yield 70%) were obtained by diffusion of diethyl ether into a dichloromethane solution. FAB mass spectrum: $m/z = 905$ ($M^+ - I$). NMR ($CDCl_3$): ^{1}H, δ 3.65, [t, 2 H, J(P–H) = 10.9 Hz, CH_2] and 7.26–7.76 (m, 20 H, Ph); ^{31}P, δ 27.2 (s).

$[Au_3(\mu\text{-tppm})Cl_3]$ 4. The complex was synthesized by a modification of the literature method.[9] A solution of tppm (0.102 g, 0.18 mmol) in dichloromethane (10 cm^3) was added dropwise to a solution of chloro(dimethyl sulfide)gold(I) (0.16 g, 0.53 mmol) in the same solvent (20 cm^3) at room temperature. Upon stirring for 1 h a white precipitate was formed. The reaction mixture was concentrated *in vacuo* to 20 cm^3, and precipitation of the product was completed by addition of pentane (50 cm^3). The crude product was recrystallized by diffusion of diethyl ether into a dichloromethane solution (yield 60%). FAB mass spectrum: $m/z = 1230$ ($M^+ - Cl$). NMR ($CDCl_3$: ^{1}H, δ 7.13–7.74 (m, 30 H, Ph) and 6.30 (s, 1 H, HCP_3); ^{31}P, δ 34.0 (s).

$[Au_3(\mu\text{-tppm})I_3]$ 5. The complex was synthesized by a modification of the literature method.[9] A suspension of KI (0.3 g, 1.8 mmol) and **4** (0.08 g, 0.1 mmol) in acetone (300 cm^3) was refluxed for 1 h and then stirred at room temperature for 24 h. The mixture was evaporated to dryness and the solid residue washed with water. The crude sample was recrystallized by dif-

fusion of diethyl ether into a dichloromethane solution (yield 68%). FAB mass spectrum: *m/z* 1413 ($M^+ - I$). NMR ($CDCl_3$): ^{1}H, δ 7.80–7.26 (m, 30 H, Ph) and 6.41 (s, 1 H, HCP_3); ^{31}P, δ 31.5 (s) [Found: C, 3.05; H, 2.40. Calc. for $C_{37}H_{31}Au_3I_3P_3\cdot(CH_3)_2CO$: C, 30.05; H, 2.35%].

[Au_3(μ-dpmp)$_2Cl_2$]Cl 6. A dichloromethane (20 cm^3) solution of dpmp (0.2 g, 0.23 mmol) was dropwise added to a solution of [AuCl(SMe_2)] (0.68 mmol, 0.2 g) in the same solvent (20 cm^3) for 1 h. The solution was concentrated to 10 cm^3. Upon diffusion of diethyl ether, yellow crystals (yield 50%) of [Au_3(μ-dpmp)$_2Cl_2$]Cl were obtained. FAB mass spectrum: *m/z* 1675 (M^+). NMR (CD_2Cl_2): ^{1}H, δ 7.77–7.10 (m, 50 H, Ph) and 3.76–3.68 [q, 8 H, *J*(P–H) = 21.0 Hz, CH_2]; ^{31}P, δ 35.186 (s) and 30.600 (s) (Found: C, 43.9; H, 3.10; Cl, 5.90. Calc. for $C_{64}H_{58}Au_3Cl_3P_6$: C, 44.95; H, 3.40; Cl, 6.20%).

[Au_3(μ-dpmp)$_2I_2$]I 7. A suspension of [Au_3(μ-dpmp)$_2Cl_2$]Cl (0.2 g, 0.12 mmol) and KI (0.08 g, 1.5 mmol) in acetone (150 cm^3) was refluxed for 1 h, and then stirred for 24 h at room temperature. The yellow solid obtained was recrystallized from acetone to give yellow needle crystals (yield 70%). FAB mass spectrum: *m/z* 1855 (M^+). NMR: ^{1}H (CD_3CN), δ 7.89–7.26 (m, 50 H, Ph) and 3.71–3.61 [q, 8 H, *J*(P–H) = 24.6 Hz, CH_2]; ^{31}P (CD_2Cl_2), δ 30.52 (s) and 27.98 (s) (Found: C, 37.8; H, 2.85; I, 18.9. Calc. for $C_{64}H_{58}Au_3I_3P_6$: C, 38.75; H, 2.95; I, 19.2%).

Instrumentation

Proton and ^{31}P NMR spectra were recorded on a Bruker DRX 500 (500 MHz) multinuclear FT-NMR spectrometer. Chemical shifts (δ in ppm) are reported relative to tetramethylsilane (^{1}H) and external H_3PO_4 (^{31}P), respectively. Mass spectra were recorded on a Finnigan MAT 95 spectrometer, UV/VIS absorption spectra on a Milton Roy Spectronic 3000 diode-array spectrophometer and steady-state emission spectra on a SPEX Fluorolog-2 spectrofluorometer. Lifetime measurements were performed with a Quanta Ray DCR-3 Nd–YAG laser (pulse output 355 nm, 8 ns). Solutions for photochemical experiments were degassed by at least four freeze–pump–thaw cycles. Low-temperature emission measurements were made with powder samples clamped by two quartz plates in an ADP DE-202 cryogenic cooler. A resistance heater was used for temperature control between 10 and 300 K. The emitted light was collected at right angles to the exciting light beam. Time-resolved emission spectra were recorded on a Princeton Instrument CCD Spectroscopic Multichannel Analyzer (CSMA) system, operated in the gated mode.

Crystallography

The structures of [Au_3(μ-tppm)I_3]·H_2O, [Au_3(μ-dpmp)$_2Cl_2$]Cl·CH_2Cl_2 and [Au_3(μ-dpmp)$_2I_2$]I·0.5Me_2CO were determined. Raw intensity data were collected at 298 K on a Rigaku AFC7R four-circle diffractometer (50 kV and 150 mA) using graphite-monochromated Mo-Kα radiation (λ 0.710 73 Å) and the ω–2θ scan mode. Intensity data (**5**, $2\theta_{max}$ = 50°, *h* 0–29, *k* 0–30, *l* −1 to 30; **6**, $2\theta_{max}$ = 45°, *h* 0–14, *k* −19 to 18, *l* −12 to 12; and **7**, $2\theta_{max}$ = 55°, *h* 0–17, *k* 0–13, *l* −25 to 24) were corrected for absorption using ψ-scan data and also for Lorentz-polarization effects. Patterson superposition yielded the positions of all non-hydrogen atoms, which were subjected to antisotropic refinement. All hydrogens except those of water were generated geometrically (C–H fixed at 0.96 Å) and allowed to ride on their respective parent C atoms; they were assigned the same isotropic thermal parameters and included in the structure-factor calculations. Computations were performed using the SDP program[10a] for **6** and the SHELTXL-PC program package[10b] for **5** and **7**. Analytic expressions of atomic scattering factors were employed, and anomalous dispersion corrections were incorporated.[11] The weighting schemes were $w = 4F_o^2/[\sigma^2(F_o^2) + 0.04(F_o^2)^2]$ for **6** and $w = [\sigma^2|F_o| + 0.0002|F_o|^2]^{-1}$ for **5** and **7**.

Details of crystal parameters, data collection and structure refinement are given in Table 1, selected bond distances and angles in Table 2.

Atomic coordinates, thermal parameters, and bond lengths and angles have been deposited at the Cambridge Crystallographic Data Centre (CCDC). See Instructions for Authors, *J. Chem. Soc., Dalton Trans.*, 1997, Issue 1. Any request to the CCDC for this material should quote the full literature citation and the reference number 186/273.

Molecular orbital calculations

Extended-Hückel molecular orbital (EHMO) calculations were carried out by using the ARGUS program.[12a] The geometry parameters were obtained from the X-ray diffraction data. The parameters of the Au atom were taken from ref. 12(*b*).

Results and Discussion

Synthesis

The syntheses of the gold(I) complexes studied are outlined in Scheme 1. The complexes [Au_2(μ-dppm)I_2] **3**, [Au_3(μ-tppm)Cl_3] **4** and [Au_3(μ-tppm)I_3] **5** have been reported previously.[7–9] The metathesis of [Au_2(μ-dppm)$_2Cl_2$] and [Au_3(μ-tppm)Cl_3] with KI in acetone readily gives **3** and **5** respectively. As expected, the ^{31}P NMR spectra of **3**–**5** show a singlet with chemical shifts consistent with the literature values.[8,9]

The reaction of [AuCl(SMe_2)] with a stoichiometric amount of dpmp in dichloromethane gave a clear yellow solution, from which [Au_3(μ-dpmp)$_2Cl_2$]Cl **6** was obtained. The complex [Au_3(μ-dpmp)$_2I_2$]I **7** was obtained by the reaction of **6** with KI. The ^{31}P NMR spectra show two singlets, at δ 35.19 and 30.60 for **6** and of δ 30.52 and 27.98 for **7**.

Crystal structures

Fig. 1 shows a perspective view of the [Au_3(μ-tppm)I_3] molecule. The structure is similar to that of [Au_3(μ-tppm)Cl_3] reported by Schmidbaur and co-workers.[9] Three Au–I units are held together by the tppm ligand and Au^I–Au^I interactions. The three Au^I form an equilateral triangular array with the Au–Au–Au angle of 60.1(1)°. The Au–Au distances average 3.136(1) Å, slightly shorter than that in [Au_3(μ-tppm)Cl_3] [3.201(1) Å]. This is in agreement with the recent work by Pyykkö *et al.*[13] that the Au^I–Au^I interaction would be enhanced with co-ordinated iodide compared with chloride. Not surprisingly, the Au^I–Au^I separations are larger than those in cationic [Au_3(μ-tppm)$_2$Cl]$^{2+}$ [2.9220(8) and 3.0889(8) Å].[3e] The I–Au–P axis is close to linear with an angle of 168.3(1)° similar to that of 172.5(1)° in [Au_3(μ-tppm)Cl_3].[8]

A perspective view of the [Au_3(μ-dpmp)Cl_2]$^+$ cation is shown in Fig. 2. The three Au^I are bridged by two dpmp ligands with the Au–P distances ranging from 2.32(1) to 2.33(1) Å. These values are comparable to those of 2.295(3)–2.315(3) Å in [Au_3(μ-dpmp)$_2$]$^{3+}$.[3f] Atom Au(2) is two-co-ordinated whereas Au(1) and Au(3) are pseudo-three-co-ordinated. The Au(3)–Cl(3) bond distance is longer than Au(1)–C(1), reflecting a stronger gold–chloride interaction at Au(1) than at Au(3). This

$$K[AuCl_4] \xrightarrow{(i)} [Au_2(\mu\text{-dppm})Cl_2] \xrightarrow{(ii)} [Au_2(\mu\text{-dppm})I_2]$$
$$[AuCl(SMe_2)] \xrightarrow{(iii)} [Au_3(\mu\text{-tppm})Cl_3] \xrightarrow{(ii)} [Au_3(\mu\text{-tppm})I_3]$$
$$[AuCl(SMe_2)] \xrightarrow{(iv)} [Au_3(\mu\text{-dpmp})_2Cl_3] \xrightarrow{(ii)} [Au_3(\mu\text{-dpmp})_2I_3]$$

Scheme 1 (*i*) 2,2′-Thiodiethanol, dppm, MeOH; (*ii*) KI, Me_2CO; (*iii*) tppm, CH_2Cl_2

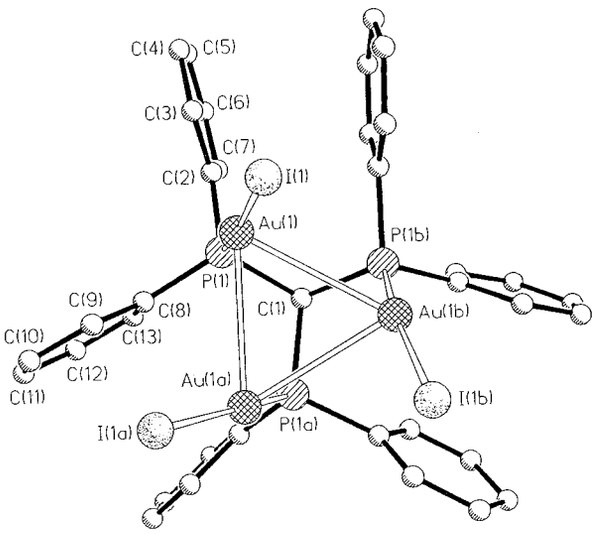

Fig. 1 Perspective view of $[Au_3(\mu\text{-tppm})I_3]$

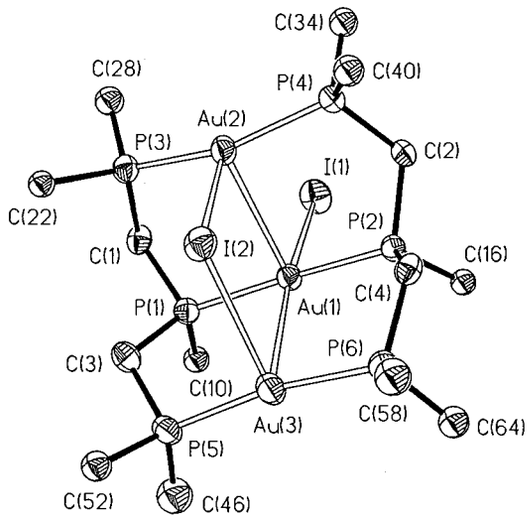

Fig. 3 Perspective view of the $[Au_3(\mu\text{-dpmp})_2I_2]^+$ cation (phenyl rings omitted)

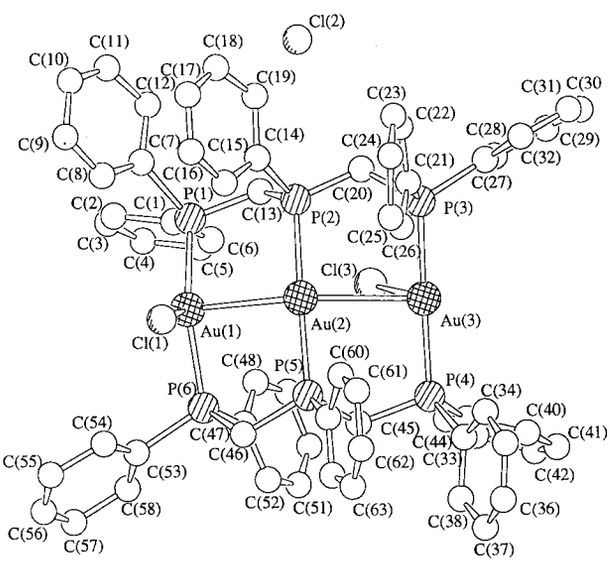

Fig. 2 Perspective view of the $[Au_3(\mu\text{-dpmp})_2Cl_2]^+$ cation

may explain the difference in the P–Au–P angles at Au(1) and Au(3). Indeed the P(3)–Au(3)–P(4) angle of 173.9(5)° is approximately linear. The Au(1)–Au(2)–Au(3) chain is bent with an angle of 149.56(9)°. This is similar to the related value of 136.26(4)° in $[Au_3(\mu\text{-dmmp})_2]^{3+}$ [dmmp = bis(dimethylphosphinomethyl)methylphosphine].[3c] The Au–Au distances of 2.946(3) and 2.963(3) Å are shorter than those of 3.0137(8) and 3.0049(8) Å in $[Au_3(\mu\text{-dpmp})_2]^{3+}$.[3f] According to Schmidbaur,[14] such intermetallic Au–Au contacts suggest the existence of weak metal–metal interactions.

A perspective view of the $[Au_3(\mu\text{-dpmp})_2I_2]^+$ cation is depicted in Fig. 3. All the gold atoms are three-co-ordinated: Au(2) and Au(3) are bridged by one iodide whereas Au(1) has a terminal iodide. The Au(2)–Au(1)–Au(3) angle of 103.5(1)° is much smaller than that of 149.56(9)° in the chloride analogue, $[Au_3(\mu\text{-dpmp})_2Cl_2]^+$. The much larger bending of the Au_3 chain is attributed to the stronger Au–Au bonding interaction, which is enhanced by the soft I^- ligand. In fact, the intramolecular Au–Au distances of 2.952(1) and 3.020(1) Å are comparable to the values of 3.0137(8) and 3.0049(8) Å in $[Au_3(\mu\text{-dpmp})_2]^{3+}$,[3f] 2.981(1) and 2.962(1) Å in $[Au_3(\mu\text{-dmmp})_2]^{3+}$ [3c] and 2.946(3) and 2.963(3) Å $[Au_3(\mu\text{-dpmp})_2Cl_2]^+$.

Spectroscopic properties

All the gold(I) complexes prepared in this work are light yellow to yellow. Their UV/VIS spectral data are summarized in Table 3. As representative examples, the absorption spectra of **6** and **7** are shown in Fig. 4. The mononuclear complex **1** displays no appreciable absorption at 300–400 nm. However, the trinuclear complexes which have Au–Au contacts less than 3.3 Å show significant absorptions at wavelengths greater than 300 nm. For example, **6** shows an intense absorption band at 356 nm and a shoulder at 326 nm while **7** shows a maximum at 320 nm with shoulders at 375 and 420 nm. We attribute this spectral feature to weak gold(I)–gold(I) interactions in the trinuclear gold(I) complexes, which cause the red-shift of the metal-centred $5d \longrightarrow 6s/6p$ transitions. Previous studies on related trinuclear gold(I) phosphine complexes $[Au_3(dmmp)_2]^{3+}$ [3c] and $[Au_3(dpmp)_2]^{3+}$ [3f] revealed that the lowest-energy allowed transitions are due to $d_{\sigma^*} \longrightarrow p_\sigma$, where d_{σ^*} is the antisymmetric combination of the $5d_{z^2}$ orbitals and p_σ is the symmetric combination of the $6p_{z^2}$ orbitals of the gold atoms.

Extended-Hückel molecular-orbital calculations on complexes **2**–**5** have been undertaken. The energy and compositions of the HOMO (highest occupied molecular orbital) and LUMO (lowest unoccupied molecular orbital) are summarized in Table 4. For **3** and **5** the HOMO has a large iodide contribution, whereas for **2** and **4** the Au 5d (96 and 95%, respectively) orbital is predominant. Changing from chloride to iodide causes a significant increase in the halide character of the HOMO. In all the complexes studied, the LUMO is the phosphine π* orbital.

Except for $[AuI(PPh_3)]$ all the gold(I) complexes display photoluminescence both in dichloromethane solution and in the solid state. The photophysical data are summarized in Table 3. At room temperature dichloromethane solutions of **2**–**7** give a broad and featureless emission band with the emission maxima ranging from 550 to 660 nm and emission lifetimes from 0.5 to 2.5 μs (Table 3). In the solid state the emissions of these gold(I) complexes are strongly affected by temperature. In general, dual emissions are observed at low temperature. The high-energy emissions, if observable, are at 480–530 nm, whereas the low-energy ones lie between 570 and 700 nm.

The temperature effect on the solid-state emissions has been studied. At room temperature the iodide complexes, **3**, **5** and **7** display only the low-energy emission, while the chloride complexes **2** and **6** show relatively weak visible emission. As representative examples, the emission spectra of **3**, **6** and **7** at various temperatures are shown in Figs. 5–7 respectively. In the assign-

Table 1 Crystallographic data

	$[Au_3(\mu\text{-tppm})I_3]\cdot H_2O$	$[Au_3(\mu\text{-dpmp})_2Cl_2]Cl\cdot CH_2Cl_2$	$[Au_3(\mu\text{-dpmp})_2I_2]\cdot 0.5(Me_2CO)$
Formula	$C_{37}H_{31}Au_3I_3P_3\cdot H_2O$	$C_{64}H_{58}Au_3Cl_3P_6\cdot CH_2Cl_2$	$C_{64}H_{68}Au_3I_3P_6\cdot 0.5(CH_3)_2CO$
M	1558.17	1795.20	2010.5
Crystal system	Cubic	Triclinic	Monoclinic
Space group	$I43d$ (no. 220)	$P\bar{1}$ (no. 2)	$P2_1/c$
Crystal size/mm	0.15 × 0.15 × 0.15	0.27 × 0.28 × 0.34	0.2 × 0.2 × 0.38
a/Å	25.274(3)	14.080(7)	18.426(4)
b/Å		19.798(4)	14.459(3)
c/Å		12.692(4)	26.597(5)
α/°		94.26(3)	
β/°		109.26(2)	105.69(3)
γ/°		103.86(4)	
U/Å^3	16 145(8)	3196(2)	6822(3)
Z	16	2	4
F(000)	11 264	1724	3764
μ/cm^{-1}	133.2	72.89	
D_c/g cm^{-3}	2.564	1.865	1.958
No. of unique reflections	1284	8375	6357
No. of data used in refinement	1113 [$(F_o) > 4\sigma(F_o)$]	2756 [$I > 2\sigma(I)$]	5329 [$(F_o) > 4\sigma(F_o)$]
No. of variables	143	372	302
Maximum transmission factors	0.642, 1.000	0.417, 0.999	0.642, 1.000
R,[a] R' [b]	0.027, 0.028	0.060, 0.057	0.034, 0.044

[a] $R = \Sigma(||F_o| - |F_c||)/\Sigma|F_o|$. [b] $R' = [\Sigma w(|F_o| - |F_c|)^2/\Sigma |F_o|^2]^{\frac{1}{2}}$.

Table 2 Selected bond distances (Å) and angles (°) of complexes **5**–**7**

Compound **5**			
Au(1)–I(1)	2.568(1)	Au(1)–P(1)	2.275(3)
Au(1)–Au(1a)	3.136(1)	Au(1)–Au(1b)	3.136(1)
I(1)–Au(1)–P(1)	168.3(1)	I(1)–Au(1)–Au(1a)	114.71
P(1)–Au(1)–Au(1a)	76.4(1)	I(1)–Au(1)–Au(1b)	88.6(1)
P(1)–Au(1)–Au(1b)	94.2(1)	Au(1a)–Au(1)–Au(1b)	60.1(1)
Compound **6**			
Au(1)–Au(2)	2.946(3)	Au(1)–Cl(1)	2.77(1)
Au(1)–P(1)	2.32(1)	Au(1)–P(6)	2.35(1)
Au(2)–Au(3)	2.963(3)	Au(2)–P(2)	2.33(1)
Au(2)–P(5)	2.32(1)	Au(3)–P(3)	2.33(1)
Au(3)–P(4)	2.32(1)	Au(3)–Cl(3)	2.84(1)
Au(2)–Au(1)–Cl(1)	78.9(3)	Au(2)–Au(1)–P(1)	93.3(3)
Au(2)–Au(1)–P(6)	89.7(3)	Au(1)–Au(2)–Au(3)	149.56(9)
Au(1)–Au(2)–P(2)	88.1(3)	P(1)–Au(1)–P(6)	147.9(5)
Au(3)–Au(2)–P(2)	92.0(3)	P(2)–Au(2)–P(5)	176.5(5)
Au(2)–Au(3)–P(3)	86.4(3)	P(3)–Au(3)–P(4)	173.9(5)
Compound **7**			
Au(1)–Au(2)	2.952(1)	Au(1)–Au(3)	3.020(1)
Au(1)–I(1)	3.008(1)	Au(1)–P(1)	2.307(3)
Au(1)–P(2)	2.316(3)	Au(2)–I(2)	3.036(1)
Au(2)–P(3)	2.310(3)	Au(2)–P(4)	2.320(3)
Au(3)–I(2)	3.191(1)	Au(3)–P(5)	2.313(4)
Au(3)–P(6)	2.316(3)		
Au(2)–Au(1)–Au(3)	103.5(1)	Au(2)–Au(1)–I(1)	85.0(1)
Au(3)–Au(1)–I(1)	171.5(1)	Au(2)–Au(1)–P(1)	88.5(1)
Au(3)–Au(1)–P(1)	86.9(1)	Au(3)–Au(1)–P(2)	86.6(1)
Au(2)–Au(1)–P(2)	90.6(1)	Au(1)–Au(2)–P(3)	94.2(1)
Au(1)–Au(2)–I(2)	77.6(1)	P(1)–Au(1)–P(2)	173.0(1)
Au(1)–Au(3)–I(2)	77.6(1)	P(3)–Au(2)–P(4)	155.3(1)
Au(2)–I(2)–Au(3)	97.7(1)	P(5)–Au(3)–P(6)	170.5(1)

Symmetry transformations: a (z, x, y); b (y, z, x).

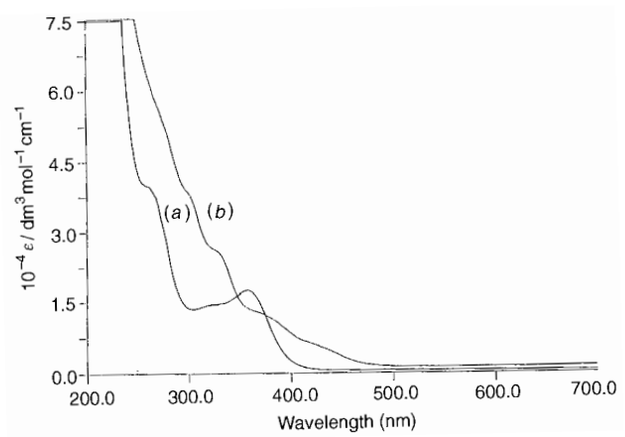

Fig. 4 The UV/VIS absorption spectra of (*a*) $[Au_3(\mu\text{-dpmp})_2Cl_2]Cl$ (1.0×10^{-5} mol dm^{-3}) and (*b*) $[Au_3(\mu\text{-dpmp})I_2]I$ (2.4×10^{-5} mol dm^{-3}) in dichloromethane at room temperature

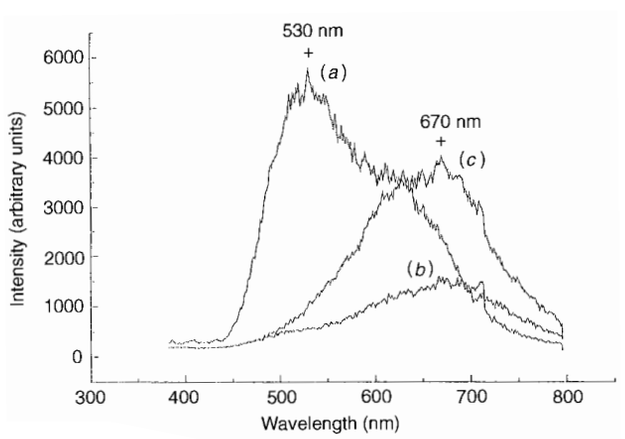

Fig. 5 Variable-temperature emission spectra of $[Au_2(\mu\text{-dppm})I_2]$ in the solid state at (*a*) 11.7, (*b*) 250 and (*c*) 292 K. Excitation at 355 nm

ment of the emission spectra the following points should be noted: (*a*) the intensities of both the high- and low-energy emissions are temperature dependent, with the latter favoured at high temperature; (*b*) the low-energy emission shows a small blue shift in energy on going from iodide to chloride; and (*c*) the excitation spectra for both the high- and low-energy emissions are the same and match the absorption spectra of the complexes. We suggest that in the chloride complexes the low-energy emission comes from the Au(d) ⟶ phosphine (π*) transition, which is modified by the metal–metal interactions. In the iodide complexes the low-energy emissions come from

Table 3 Photophysical data for gold(I) halide complexes in degassed dichloromethane at room temperature and in the solid state

Compounds	Au–Au/Å	λ_{abs}/nm (ε/dm^3 mol^{-1} cm^{-1})	λ_{em}/nm (τ_0/μs)* [Φ_{em}]*	λ_{em}/nm in the solid state
1		275 (3.4×10^3)		
2	3.351	268 (1.02×10^4)	585 (0.5)	
		300 (sh) (3.08×10^3)	[4.01×10^{-3}]	12 K: 500
				270 K: 510, 680
3		268 (1.51×10^4)	615 (1.1)	12 K: 620 (sh), 530
		300 (sh) (3.77×10^3)	[1.32×10^{-2}]	298 K: 670
4	3.201	275 (0.97×10^4)	550 (1.1)	298 K: 510, 680
		300 (sh) (0.51×10^4)	[8.5×10^{-3}]	20 K: 500
				298 K: 640
5	3.136	275 (1.39×10^4)	590 (1.2)	12 K: 480, 680
		300 (sh) (0.80×10^4)	[1.75×10^{-2}]	298 K: 680
6	2.946	260 (3.37×10^4)	650 (1.2)	77 K: 485, 620
	2.963	326 (sh)	[8.80×10^{-3}]	
		356 (1.49×10^4)		
7	2.952	295 (2.94×10^4)	660 (2.5)	12 K: 575, 665
	3.02	320 (2.05×10^4)	[2.4×10^{-2}]	
		360 (1.03×10^4)		
		420 (sh) (4.78×10^3)		

* In dichloromethane solution at room temperature.

Table 4 Components of HOMO and LUMO for gold(I) halide complexes **2**–**5** calculated by the EHMO method

	% Metal (d)		% Halide (p)		% Ligand	
Compound	HOMO	LUMO	HOMO	LUMO	HOMO	LUMO
2	95.95	0.27	2.10	0.05	1.95	99.68
3	24.74	0.13	74.61	0.07	0.66	99.80
5	32.87	0.15	66.40	0.07	0.74	99.78
4	94.84	0.18	1.71	0.02	3.45	99.80

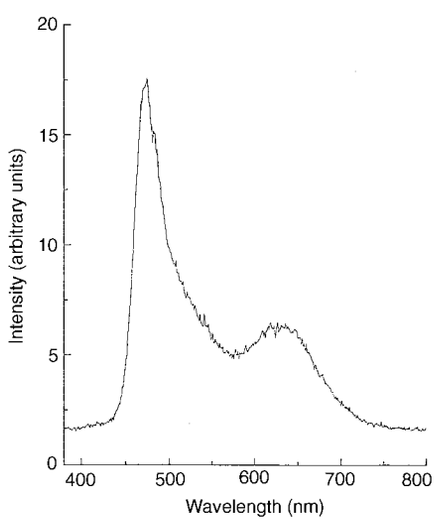

Fig. 6 Emission spectrum of $[Au_3(\mu\text{-dpmp})_2Cl_2]Cl$ in the solid state at 77 K. Excitation at 355 nm

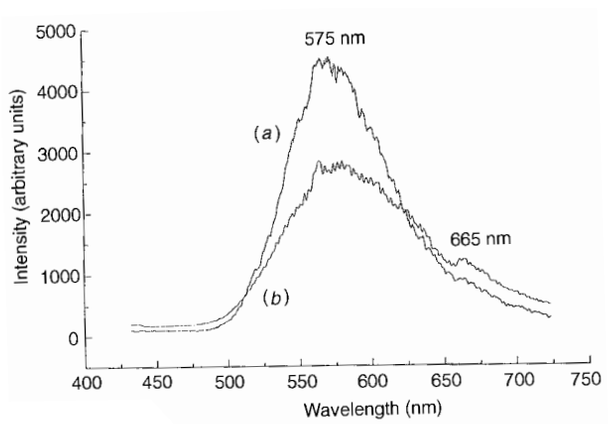

Fig. 7 Variable-temperature emission spectra of $[Au_3(\mu\text{-dpmp})_2I_2]I$ in the solid state at (*a*) 12 and (*b*) 250 K. Excitation at 355 nm

excited states which have substantial $I^- \rightarrow$phosphine (π^*) charge-transfer character. The EHMO calculations are also consistent with this assignment. As mentioned in the previous section, the HOMO of the gold(I) complexes have increased halide contribution from chloride to iodide. We denote the excited states for the low-energy emissions as ^{3}m.m.l.c.t./^{3}l.l.c.t. Here, m.m.l.c.t. means metal–metal (d_{σ^*}) to ligand (phosphine) charge transfer and l.l.c.t. ligand (halide) to ligand (phosphine) charge transfer. Recently, Fackler and co-workers[4d] reported the temperature-dependent photoluminescence of 1,3,5-triaza-7-phosphaadamantane complexes of gold, which show multiple-state emissions originating from thermally non-equilibrated excited states. The excited states for the high-energy emissions could have mixed character involving both intraligand (i.l.) and m.l.c.t. [Au $\longrightarrow$ π^*(phosphine)] transitions, and the excited states are represented by ^{3}i.l./^{3}m.l.c.t. A scheme for intersystem energy crossing between the ^{3}i.l./^{3}m.l.c.t. and the ^{3}m.m.l.c.t./^{3}l.l.c.t. states can be constructed (Fig. 8). As shown, when the temperature is raised, curve-crossing between ^{3}i.l./^{3}m.l.c.t. and ^{3}m.m.l.c.t./^{3}l.l.c.t. states might occur. We anticipate that the ^{3}m.m.l.c.t./^{3}l.l.c.t. state could be thermally populated from the high-energy state by overcoming the crossing barrier, and hence the low-energy emission is favoured at high temperature. This may account for the observed luminescence thermochromism.

Study of the variable-temperature emission spectra reveals that luminescence thermochromism is more pronounced in the iodide complexes. The well resolved high- and low-energy emission bands of **3** guarantee independent measurement of the emission lifetimes for the two excited states. It is expected that these excited states would be coupled at high temperatures, at which they will be thermally equilibrated and decay at the same rate. The lifetimes for the two excited states plotted against temperature are shown in Fig. 9. As shown, the lifetimes of the

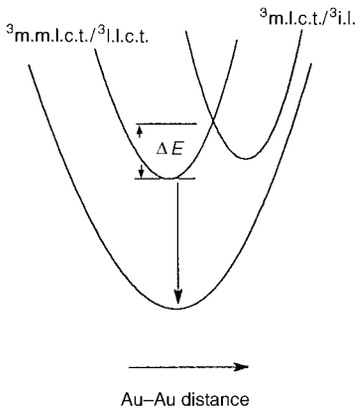

Fig. 8 Proposed model for the potential curve-crossing between ^{3}m.l.c.t./^{3}i.l. and ^{3}m.m.l.c.t./^{3}l.l.c.t., where state ΔE is the activation energy for the crossing barrier

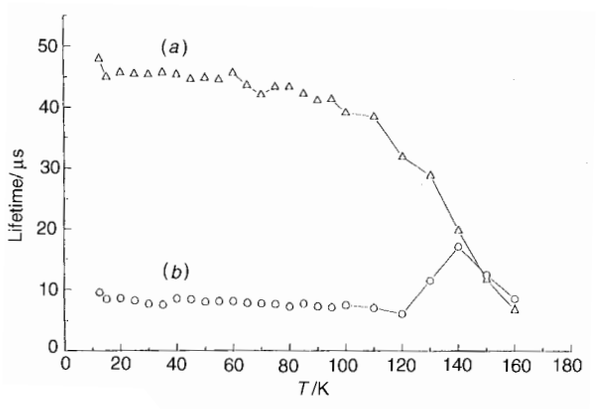

Fig. 9 Emission lifetimes recorded at various temperatures and monitored at (*a*) 530 and (*b*) 680 nm for $[Au_2(\mu\text{-dppm})I_2]$

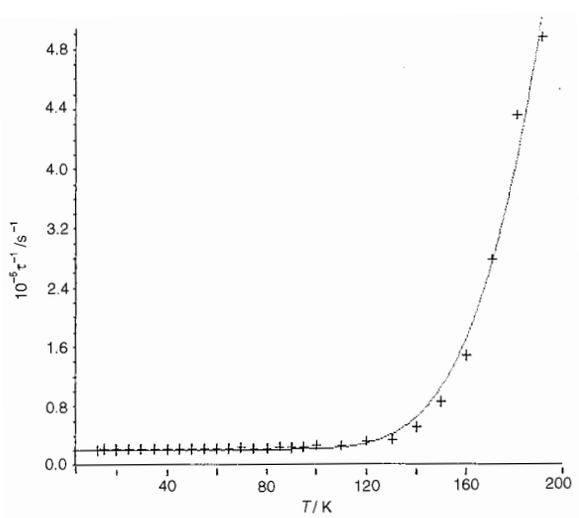

Fig. 10 Variation in the decay of the high-energy emission of $[Au_2(\mu\text{-dppm})I_2]$ as a function of temperature between 10 and 200 K

two excited states are different at temperatures below 120 K and become the same at above 140 K. This clearly demonstrates that the two states responsible for the high- and low-energy emissions poorly couple at low temperatures. A plot of emission lifetimes *vs.* temperature for **3** measured at 530 nm is shown in Fig. 10. When the temperature is below 110 K there is little change in the lifetime with temperature. However, at temperatures >110 K a dramatic decrease in lifetime is observed. The temperature at which the dramatic change occurs coincides with that for the appearance of the low-energy emission. The observed rate constants were analysed by equation[16] (1) based

$$k_p = (k_1 + k_2\, e^{-\Delta E/RT})/(1 + e^{-\Delta E/RT}) \quad (1)$$

on the assumption that the emissions originate from two thermally equilibrated levels with temperature-independent rate constants. The fitting of the rate constants *vs.* temperature is shown in Fig. 10, and the empirically derived parameters are $k_1 = 2 \times 10^4$ s^{-1}, $k_2 = 8 \times 10^8$ s^{-1} and $\Delta E = 945 \pm 45$ cm^{-1}. The energy gap can be interpreted as the energy barrier for curve-crossing, as shown in Fig. 8. It is interesting that a similar activation energy (990 ± 370 cm^{-1}) has previously been reported for tetranuclear copper(I) bromide complexes.[17]

Acknowledgements

We acknowledge support from the University of Hong Kong and The Hong Kong Research Grants Council.

References

1 P. C. Ford and A. Vogler, *Acc. Chem. Res.*, 1993, **26**, 220.
2 A. Vogler and H. Kunkley, *Chem. Phys. Lett.*, 1989, **158**, 74; C. M. Che, H. K. Yip, D. Li, S. M. Peng, G. H. Lee, Y. M. Wang and S. T. Liu, *J. Chem. Soc., Chem. Commun.*, 1991, 1615; D. M. Knotter, H. L. van Maanen, D. M. Grove, A. L. Spek and G. van Koten, *Inorg. Chem.*, 1991, **30**, 3309.
3 (*a*) C. M. Che, H. L. Kwong, V. W. W. Yam and C. K. Cho, *J. Chem. Soc., Chem. Commun.*, 1989, 855; (*b*) C. M. Che, H. L. Kwong, V. W. W. Yam and C. K. Poon, *J. Chem. Soc., Dalton Trans.*, 1990, 3215; (*c*) V. W. W. Yam, T. F. Lai and C. M. Che, *J. Chem. Soc., Dalton Trans.*, 1990, 3747; (*d*) C. M. Che, W. T. Wong, T. F. Lai, H. L. Kwong, C. K. Poon and V. W. W. Yam, *J. Chem. Soc., Dalton Trans.*, 1992, 2445; (*e*) C. M. Che, H. K. Yip, V. W. W. Yam, P. Y. Cheung, T. F. Lai, S. J. Shieh and S. M. Peng, *J. Chem. Soc., Dalton Trans.*, 1992, 427; (*f*) D. Li, C. M. Che, S. M. Peng, S. T. Liu, Z. Y. Zhou and T. C. W. Mak, *J. Chem. Soc., Dalton Trans.*, 1993, 189; (*g*) H. Xiao, K. K. Cheung, C. X. Guo and C. M. Che, *J. Chem. Soc., Dalton Trans.*, 1994, 1867.
4 (*a*) C. King, J. C. Wang, S. Wang, M. N. I. Khan and J. P. Fackler, jun., *Inorg. Chem.*, 1988, **27**, 1672; (*b*) C. King, M. N. I. Khan, R. J. Staples and J. P. Fackler, jun., *Inorg. Chem.*, 1992, **31**, 3236; (*c*) J. P. Fackler, jun., B. Assmann, K. Angermaier and H. Schmidbaur, *Inorg. Chem.*, 1995, **34**, 75; (*d*) Z. Assefa, B. G. McBurnett, R. J. Staples and J. P. Fackler, jun., *Inorg. Chem.*, 1995, **34**, 4965; (*e*) J. M. Forward, D. Bohmann, J. P. Fackler, jun. and R. J. Staples, *Inorg. Chem.*, 1995, **34**, 6330.
5 H. K. Yip, A. Schier, J. Riede and H. Schmidbaur, *J. Chem. Soc., Dalton Trans.*, 1994, 2333; T. M. McCleskey and H. B. Gray, *Inorg. Chem.*, 1992, **31**, 1733.
6 R. Appel, K. Geisler and H. F. Schöler, *Chem. Ber.*, 1979, **112**, 648.
7 K. C. Dash and H. Schmidbaur, *Chem. Ber.*, 1973, **106**, 1221.
8 H. Schmidbaur, A. Wohlleben, F. Wagner, O. Orama and G. Huttner, *Chem. Ber.*, 1977, **110**, 1748.
9 A. Stützer, P. Bissinger and H. Schmidbaur, *Chem. Ber.*, 1992, **125**, 367.
10 (*a*) SDP Structure Determination Package, Enraf-Nonius, Delft, 1985; (*b*) G. M. Sheldrick, in *Crystallographic Computing 3*, eds. G. M. Sheldrick, C. Krüger and R. Goddard, Oxford University Press, New York, 1985, p. 175.
11 J. A. Ibers and W. C. Hamilton (Editors), *International Tables for X-Ray Crystallogaphy*, Kynoch Press, Birmingham, 1974, vol. 4, p. 55, 149.
12 (*a*) M. A. Thompson, ARGUS, A Quantum Chemical Electronic Structure Program, *Version 1.1 User Manual*, Pacific Northwest Laboratory, Richland, WA, 1992; (*b*) L. C. Porter, M. N. I. Khan, C. King and J. P. Fackler, jun., *Acta Crystallogr., Sect. C*, 1989, **45**, 947.
13 P. Pyykkö, J. Li and N. Runeberg, *Chem. Phys. Lett.*, 1994, **218**, 133.
14 H. Schmidbauer, *Gold Bull.*, 1990, **23**, 11.
15 K. R. Klye, W. E. Palke and P. C. Ford, *Coord. Chem. Rev.*, 1990, **97**, 35.
16 W. A. Fordyce, H. Rau, M. L. Stone and G. A. Crosby, *Chem. Phys. Lett.*, 1981, **77**, 404.
17 C. K. Ryu, M. Vitale and P. C. Ford, *Inorg. Chem.*, 1993, **32**, 869.

Received 27*th August* 1996*; Paper* 6/05911B